Cell

Network Crosstalk Dynamically Changes during Neutrophil Polarization

Chin-Jen Ku,[1,3] Yanqin Wang,[1,3] Orion D. Weiner,[2] Steven J. Altschuler,[1,*] and Lani F. Wu[1,*]
[1]Department of Pharmacology, Green Center for Systems Biology, Simmons Cancer Center, University of Texas Southwestern Medical Center, Dallas, TX 75390, USA
[2]Cardiovascular Research Institute and Department of Biochemistry, University of California, San Francisco, San Francisco, CA 94158, USA
[3]These authors contributed equally to this work
*Correspondence: steven.altschuler@utsouthwestern.edu (S.J.A.), lani.wu@utsouthwestern.edu (L.F.W.)
DOI 10.1016/j.cell.2012.03.044

SUMMARY

How complex signaling networks shape highly coordinated, multistep cellular responses is poorly understood. Here, we made use of a network-perturbation approach to investigate causal influences, or "crosstalk," among signaling modules involved in the cytoskeletal response of neutrophils to chemoattractant. We quantified the intensity and polarity of cytoskeletal marker proteins over time to characterize stereotyped cellular responses. Analyzing the effects of network disruptions revealed that, not only does crosstalk evolve rapidly during polarization, but also that intensity and polarity responses are influenced by different patterns of crosstalk. Interestingly, persistent crosstalk is arranged in a surprisingly simple circuit: a linear cascade from front to back to microtubules influences intensities, and a feed-forward network in the reverse direction influences polarity. Our approach provided a rational strategy for decomposing a complex, dynamically evolving signaling system and revealed evolving paths of causal influence that shape the neutrophil polarization response.

INTRODUCTION

A central challenge in biology is to determine how information is dynamically transduced through signaling networks (Amit et al., 2009; Cheong et al., 2011; Levine et al., 2006; Muzzey et al., 2009; Sachs et al., 2005; Yu et al., 2008). Signaling networks are often cast as highly complex, static structures that contain many components and interactions inferred by combining results from diverse assays. One approach for studying how these networks process information is to combine detailed biochemical measurements with mathematical analyses and modeling (Kalir and Alon, 2004; Kentner and Sourjik, 2009; Lee et al., 2003; Marco et al., 2007; Oleksiuk et al., 2011). Such studies illuminate the contribution of each component in shaping the responses of the other components. However, obtaining sufficient biochemical constants required for accurate, physical models of complex networks can be difficult. Complete sets of measurements typically do not exist, and it is often not obvious which biochemical properties of the individual components have the strongest influence on the output of the system.

An alternative approach for characterizing signal processing is to quantify the effects of perturbations to network components (Janes et al., 2006; Muzzey et al., 2009; Natarajan et al., 2006; Sachs et al., 2005; Schneider and Haugh, 2006; Tkachenko et al., 2011). Perturbation analyses have enabled inference of causal network structure, including the reconstruction of a static, causal protein-signaling network in T cells (Sachs et al., 2005) and the characterization of dynamic crosstalk induced by costimulation with multiple growth factors in epithelial cells (Janes et al., 2006). As with epistasis experiments in genetics, causal interactions can be uncovered without requiring detailed biochemical mechanism or proximity within the network of components.

Neutrophils—innate immune cells that detect, hunt, and kill bacteria—offer an ideal system for studying dynamic signal processing. The polarity network of neutrophils responds rapidly to chemoattractant. Upon stimulation with f-Met-Leu-Phe (fMLP), neutrophils undergo a rapid, highly stereotyped progression through distinct stages: cells initiate polarization within seconds, develop polarization within 2–3 min, and then maintain their polarized state for about 10 min before adapting (Zigmond et al., 1981; Zigmond and Sullivan, 1979). Transitions among these different stages could reflect changes in the underlying composition of the polarity network. For example, different phases of the cellular differentiation or cell cycle are due, in part, to the synthesis and degradation of key regulatory components (de Lichtenberg et al., 2005; Fraser and Germain, 2009; Loose et al., 2007; Luscombe et al., 2004). However, for the rapid timescale of neutrophil polarization, this multiphasic response is unlikely to be guided simply by the appearance or disappearance of network components.

Many components and interactions that are involved in this neutrophil polarity network have been identified and placed within a small number of spatially and molecularly distinct cytoskeletal "modules" (Niggli, 2003; Servant et al., 2000; Small et al., 2002; Srinivasan et al., 2003; Van Keymeulen et al., 2006; Weiner et al., 2002, 2006; Wong et al., 2006, 2007; Xu et al., 2003, 2005). These include a front module that promotes membrane protrusion in the direction of the chemoattractant through

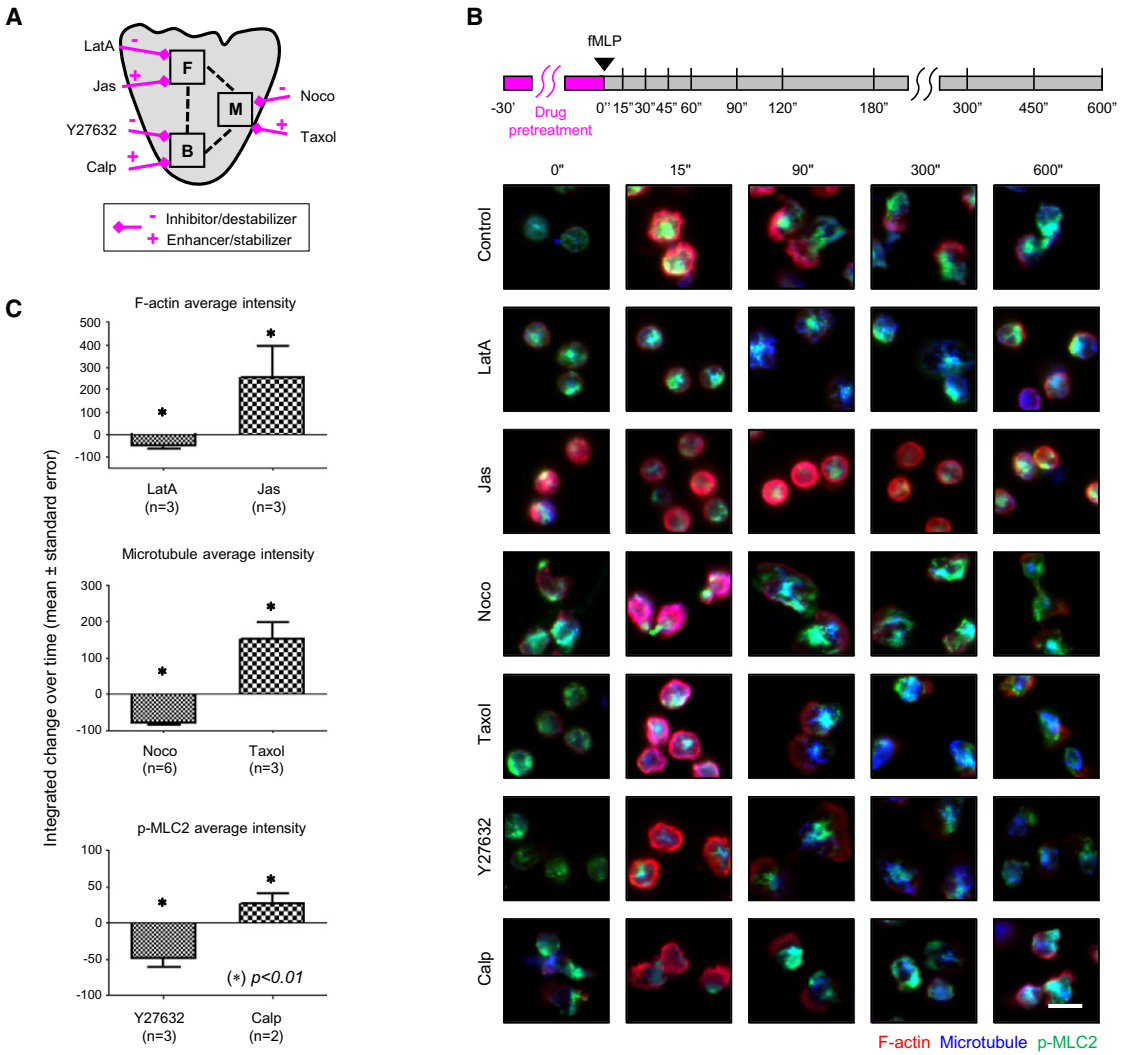

Figure 1. Pharmacological Perturbations of Key Modules in the Human Neutrophil Polarity Network

(A) Simplified schema of the polarity signaling network in primary human neutrophils containing the front (F), back (B), and microtubule (M) modules. Two opposing drug perturbations were chosen to disrupt each of the three modules: latrunculin A (LatA) and jasplakinolide (Jas) for the front; nocodazole (Noco) and taxol (Taxol) for the microtubules; and Y27632 (Y27632) and calpeptin (Calp) for the back.

(B) Cells were treated for 30 min with drugs, stimulated with 10 nM fMLP, and fixed at multiple time points. Shown are representative images of human neutrophils at different time points after fMLP stimulation. Color: red (F-actin), blue (microtubule), and green (p-MLC2). Scale bar, 10 μm.

(C) Quantification of opposing drug effects on their targeted modules. Bar graphs show fold change of overall response to drug perturbation (mean ±SE across replicate experiments; Supplemental Information).

See also Figure S1.

F-actin assembly at the leading edge of the cell; a back module that regulates cell contraction through activation of myosin light chain 2 (MLC2) at the rear end; and a module that consists of microtubules and associated proteins that is thought to act both as a sink and delivery system for several polarity components (Figures 1A and S1 available online). These modules provide a tractable starting point for exploring causal interactions, or "crosstalk," between distinct biochemical networks that produce a complex behavioral phenotype.

Numerous routes of communication between these cytoskeletal modules have been identified (front to back, front to microtubules, microtubules to back, and back to front). The front recruits the SCAR/WAVE complex, which not only shapes the actin architecture at the leading edge but also acts as a scaffold for inhibitors of the Rho/myosin back program (Weiner et al., 2006). Likewise, the back program opposes the actin-based membrane protrusions that are necessary to support leading-edge activities (Weiner et al., 2007). The microtubule module delivers Rho family guanine nucleotide exchange factors (GEFs) to the membrane to locally activate the Rho/myosin back program (Krendel et al., 2002; Odell and Foe, 2008; Xu et al., 2005), and actin polymerized at the leading edge locally

excludes microtubules (Eddy et al., 2002). How this crosstalk occurs in space and time to give rise to a rapid, multiphasic response in neutrophils is poorly understood.

Here, we investigated paths of communication between front, back, and microtubule modules in stimulated, primary human neutrophils by using a network-perturbation approach. We made use of quantitative microscopy and fixed-cell assays over multiple time points to capture the spatiotemporal dynamics of $\sim 10^5$ polarizing neutrophils. We labeled cells with three cytoskeletal marker proteins that served as proxies (or direct readouts) for the states of the front, back, and microtubule modules. For each marker, we measured two phenotypes to capture its activity levels or spatial distribution. To identify crosstalk among the modules, populations of neutrophils were treated with pharmacological perturbations before stimulation. Six mechanistically distinct drugs were selected, with pairs of these drugs targeting each of the three modules with opposite effects. This approach allowed us to capture crosstalk between modules by quantifying the degree to which perturbed response curves for marker activity levels and spatial distributions deviated from control. Our analysis revealed that crosstalk interactions differ across different phases of polarization. Further, crosstalk is different for activity and spatial distribution of the signaling markers, with persistent crosstalk arranged in a surprisingly simple circuit: a linear cascade from front to back to microtubule modules influences intensities, and a feed-forward network in the reverse direction influences polarity.

RESULTS

Measurement of Polarization Responses in Primary Human Neutrophils

We chose to analyze polarization responses in primary human neutrophils due to their physiological relevance and lower cell-to-cell variability as compared with cultured cell lines. Given the experimental challenges of measuring live readouts of signaling activities in these short-lived cells, we inferred the phenotypic responses of neutrophils based on statistics collected from populations of cells fixed at different time points. Freshly harvested human neutrophils were seeded onto 96-well plates followed by 30 min treatment of drug or control vehicle (dimethylsulfoxide [DMSO]). After uniform stimulation of chemoattractant fMLP (10 nM), cells were fixed at 11 time points ranging from 0–600 s. The time points were chosen nonuniformly to capture different phases of the polarization process (Figure 1B, top; Supplemental Information).

We costained cells for F-actin, monophosphorylated MLC2 (p-MLC2), and α-tubulin to obtain integrated signaling readouts of front, back, and microtubule modules, respectively (Figure 1B, bottom). F-actin assembly at the front is the engine for leading edge advance and represents a proxy for upstream signals (like Rac activation) that control protrusion. Phosphorylation of MLC2 activates the contractile ability of myosin and is a proxy for upstream signals (like Rho activation) that activate trailing edge contraction. The microtubule module is both a sink and delivery system for polarity components; the mass and spatial distribution of microtubules is thought to regulate neutrophil polarity. In addition to these primary readouts, we also stained neutrophil nuclei (Hoechst) and acquired bright field microscopy images to perform image segmentation and image quality control (Ku et al., 2010).

To identify individual cellular regions from microscopy images, we made use of our previously developed image segmentation algorithm (Ku et al., 2010). After intensity normalization (Supplemental Information; Figure S2A), we extracted two phenotypes for each marker on a cell-by-cell basis. First, we measured the average intensity of each marker to capture an integrated activity level of its associated module. For example, a high value of F-actin intensity indicated high levels of front activity. Second, we measured the polarity of each marker to capture the spatial extent of the most active signaling region. More specifically, polarity measured how tightly packed the brightest pixels were inside of the cell (Supplemental Information) (Ku et al., 2010). For example, uniform actin staining gives a low value for F-actin polarity, whereas tight concentration of actin at the leading edge gives a high value for F-actin polarity. Similarly, the higher the value of polarity for p-MLC2 or microtubules, the tighter their spatial distribution is.

To perturb each module in the neutrophil polarity network, we made use of pairs of pharmacological compounds with opposite effects (Figures 1A and 1B): the F-actin depolymerizer latrunculin A (LatA) or stabilizer jasplakinolide (Jas) to perturb the front module, the microtubule depolymerizer nocodazole (Noco) or stabilizer taxol (Taxol) to perturb the microtubule module, and the myosin phosphorylation inhibitor Y27632 or activator calpeptin (Calp) to perturb the back module. Drug concentrations were chosen by serial titration assays to be strong enough to induce a noticeable effect on primary target activity yet sufficiently small to minimize cytotoxic effects (Figures S1B–1D). Analysis of the intensity response of the drug-targeted readouts clearly showed the expected opposing effects of these drug perturbations (Figure 1C).

Together, these experiments captured a collection of data points that are far too large to examine by eye. To identify circuits controlling cellular behavior, we designed an analysis approach to quantify and summarize this data. We next describe our steps for constructing dynamic response curves from the time course data, constructing deviation profiles by quantifying how perturbed response curves varied from control and constructing crosstalk diagrams and causal networks from the deviation profiles.

Dynamic Response Curves

We first developed a robust approach for summarizing the dynamics of the polarization response that was observed for large numbers of neutrophils. For each replicate experiment, a population median was estimated for each condition (control or perturbation), marker (F-actin, p-MLC2, or microtubule), phenotype (intensity or polarity), and time point (Supplemental Information). Next, by interpolating these medians across the 11 time points, we obtained response curves for each replicate, condition, marker, and phenotype (Supplemental Information). Finally, representative response curves were obtained by taking medians across all replicates. Together, these response curves

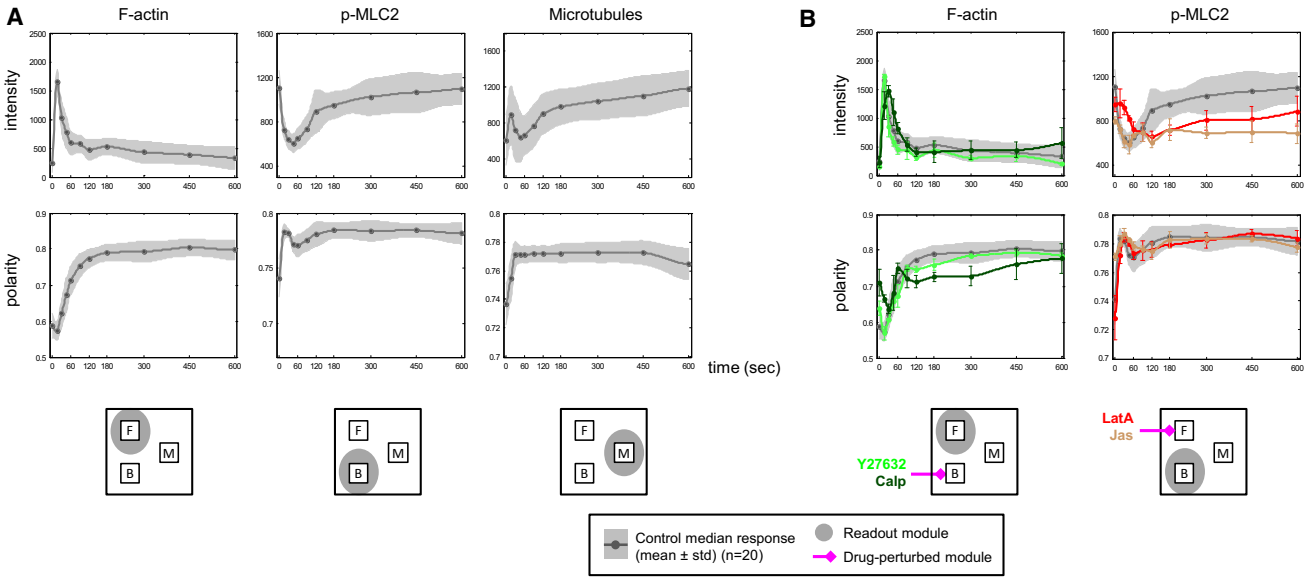

Figure 2. Dynamic Responses of Neutrophils to Drug Perturbations

(A) Neutrophil response curves for front (left), back (middle), and microtubule (right) intensity (top row) and polarity (bottom row) phenotypes. Dark-gray curve represents the mean of median response across replicates (n = 20). Gray band represents one SD above and below the mean values.

(B) Response of front module to perturbations of the back (left) or response of back module to perturbations of the front (right) for intensity (top) and polarity (bottom) phenotypes. Color curves represent the mean of population median responses (red/brown, front perturbations; bright/dark green, back perturbations). Error bars represent SEM of median drug responses at different time points.

See also Figure S2.

provided temporal characterizations of how the intensity or polarity phenotypes of different module readouts changed upon fMLP stimulation in control or perturbed conditions (Figures 2A and S2C).

As multiple batches of primary human neutrophils had been assayed over a period greater than a year, a concern was whether the time-varying responses of neutrophil polarization had remained consistent and reproducible. To assess this variability, we first investigated the control responses of neutrophils to fMLP from 20 replicates taken across all batches of experiments. We focused first on analyzing the F-actin intensity response and morphological elongation, which are classic measurements of neutrophil responses to chemoattractant. The resulting response curves showed expected increases in actin polymerization and morphological elongation after stimulation. Importantly, the collection of response curves showed remarkably consistent trends from experiment to experiment (Figure S2B). Next, for each phenotype and marker, we examined variability among our 20 replicate control response curves as measured by SD (Figure S2C, light gray shaded regions) around the mean of the median response curves (Figure S2C, dark gray lines). Again, we observed a high degree of agreement among replicate response curves for each phenotype and marker. Taken together, these results demonstrated that our experimental and computational approach produced consistent and reproducible phenotypes from different batches of polarizing primary human neutrophils. Our control response curves provided a baseline for subsequent investigation of the time-varying effects of perturbing the polarity network.

Response Dynamics Depends on Phenotype

As was apparent from examining the response curves, the intensity and polarity phenotypes could have dramatically different dynamic behaviors, even for the same marker. For example, the control response curves for front and back intensity returned to near-prestimulation levels, whereas those for polarity did not. The intensity of microtubules continued to increase over the duration of the 600 s observation (consistent with classic studies [Schliwa et al., 1982]), whereas polarity stabilized after only 60 s (Figure 2A).

Next, we observed that some perturbations yielded different phenotypic consequences for the intensity versus polarity of the same marker (Figure 2B). For example, Calp perturbation to the back module strongly affected the polarity, but not the intensity, of the front (Figure 2B, left column; dark green drug perturbation curve outside gray control region). Conversely, LatA and Jas perturbations to the front module strongly affected the intensity, but not the polarity, of the back (Figure 2B, right column). The difference in response curves between intensity and polarity suggested that crosstalk between modules may be phenotype dependent.

Deviation Profiles

We next quantified the degree to which perturbed response curves deviated from control. First, to begin summarizing our large data set, we partitioned our 10 min observation time into five time intervals: a first time interval of 1 min to capture initial fast responses and four subsequent time intervals, spaced ~2 min apart, to capture later responses (Figure 3A). Second,

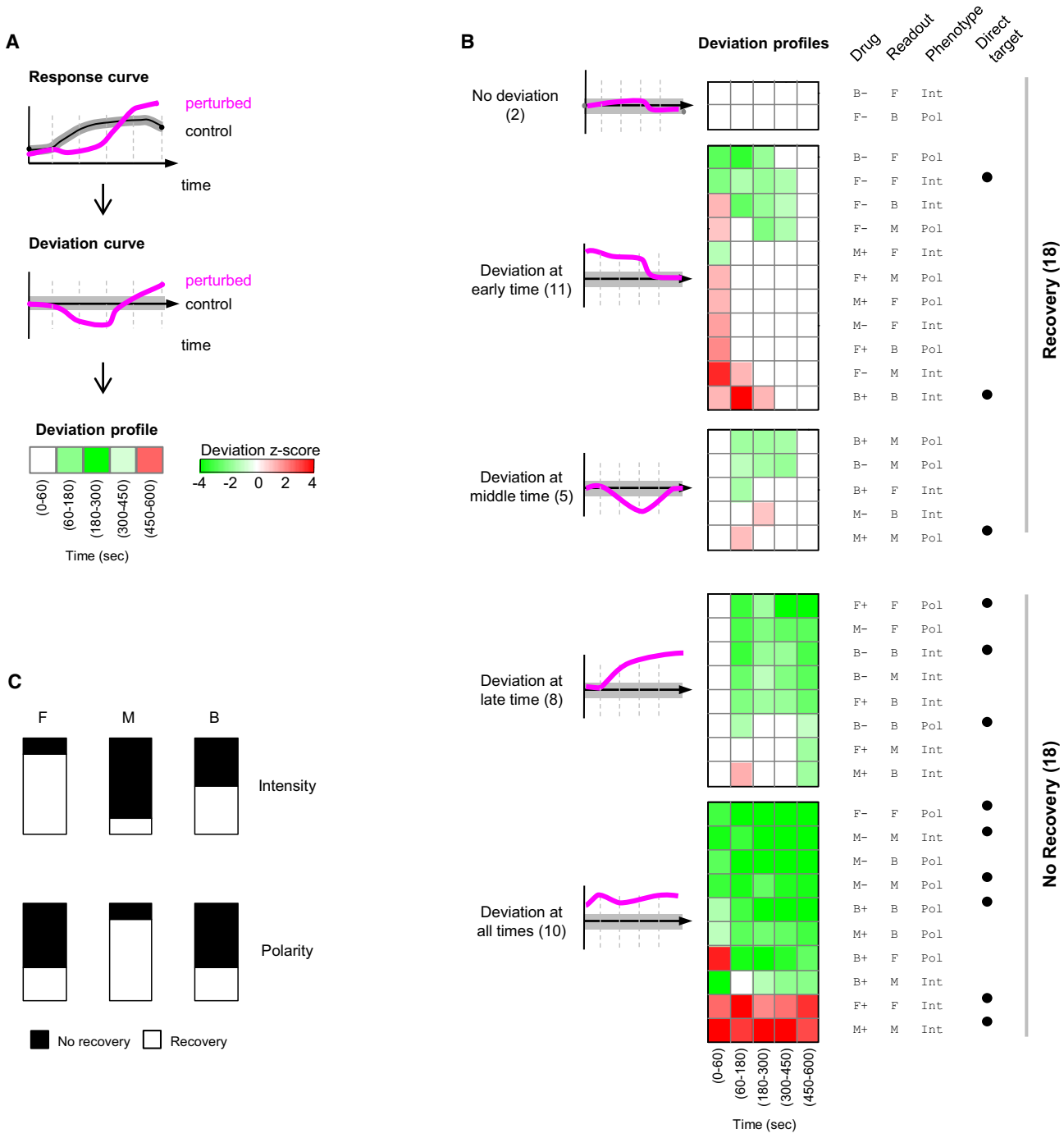

Figure 3. Deviation Profiles Summarized Dynamics of Perturbation Effects

(A) Illustration of how deviation profiles were generated by quantifying drug-induced deviations to control response curves at different time intervals (0–1, 1–3, 3–5, 5–7.5, and 7.5–10 min) (Supplemental Information). Color map, red/white/green (significantly increased/unchanged/decreased feature value).

(B) Deviation profiles across phenotypes and perturbations (heat map) showed various temporal patterns: deviation at no time, early time, middle time, late time, or all times (cartoon illustrations at left; Supplemental Information). Deviation profiles were further grouped depending on whether the deviation disappeared by (i.e., recovery) or persisted through (i.e., no recovery) the end of the polarization process. Numbers next to different labels represented the number of deviation profiles exhibiting the corresponding patterns.

(C) Distribution of deviation profiles of front, microtubule, and back modules based on their ability to recover (recovery, white; nonrecovery, black). Top shows intensity phenotype. Bottom shows polarity phenotype.

as a robust measure of the deviation of a phenotypic response, for each time interval, we measured the area difference between a drug-perturbed response curve and its corresponding control response curve from the same experiment (i.e., 96-well plate). Third, to determine statistical significance, we turned this area difference into a dimensionless z score by comparing the drug-induced deviation to variation among replicate controls (Figure S2D; Supplemental Information) (Natarajan et al., 2006; Perlman et al., 2004). A positive or negative z score signified an increased or decreased drug response, respectively. Fourth, we combined z scores over different time intervals to construct a deviation profile. These profiles provided a compact summary of when or whether a perturbed response curve deviated from and/or returned to the control response (Figure 3A).

We observed a spectrum of deviation dynamics, including response curves that never or always deviated, as well as curves that deviated only at early, middle, or late times from control response (Figure 3B; Supplemental Information). As expected, most deviation profiles associated with directly targeted modules (e.g., LatA/Jas on F-actin; Figure 3B, black dots at right; Figure 2B, response curves) showed no recovery, with deviations that largely persisted throughout the process of polarization (9 out of 12 direct targets). On the other hand, the majority of deviation profiles that showed recovery were associated with nondirectly targeted modules (15 out of 18 deviation profiles). Interestingly, the majority of positive deviation profiles (in red) were transient, showing deviation only at early times, whereas the majority of negative deviation profiles (in green) showed no recovery, though to a lesser degree. We further analyzed the distribution of deviation profiles based on their ability to recover at the end of the observation time. We found that the front intensity had the highest recovery rate, whereas microtubule intensity had the least recovery rate. Interestingly, this trend was reversed for polarity, with microtubule polarity having the highest recovery rate (Figure 3C). These results suggested that front intensity and microtubule polarity are the least likely to be persistently affected by perturbations to the other modules, whereas the situation is reversed for front polarity and microtubule intensity.

From Deviation Profiles to Network Crosstalk

To capture intermodule influence on shaping response curves, we next made use of the deviation profiles to determine when the phenotypic response curve of a module deviated significantly from control. Network crosstalk was visualized by combining all of the deviation profiles associated with each perturbation (Figure 4). For each perturbation and time interval, we created a diagram in which modules were colored by their deviation z scores. Arrows from directly to nondirectly targeted modules were drawn and colored (grayscale) to indicate crosstalk if significant deviations of intensity or polarity were found (Supplemental Information). That is, a link was drawn from module 1 to module 2 at time *t* if stimulation with fMLP in the presence of a perturbation to module 1 causes a change to a specified phenotype of module 2 at time *t*. This approach is similar in spirit to epistasis studies in genetics, in which phenotypes are measured in the presence or absence of a pre-existing perturbation.

The network diagrams revealed time- and phenotype-dependent crosstalk. For example, the back inhibitor Y27632 affected front polarity at early times, but not later times, yet affected microtubule intensity at later, but not early, times. Satisfyingly, when and where both of the paired perturbations (i.e., LatA/Jas, Noco/Taxol, or Y27632/Calp) induced significant crosstalk, the observed deviations to nondirectly targeted modules were largely consistent. For example, both microtubule drugs induced negative deviations to back polarity. The consistency of perturbation effects, despite using drugs of different mechanisms, supported the assumption that observed crosstalk was due to perturbation of the targeted module (Supplemental Information). Our network diagrams provided an intuitive, perturbation-based, and module-centric visualization of how crosstalk evolved in time and varied by phenotype.

Intriguingly, for several of the crosstalk links, either activation or inhibition of one module decreased activation of another module. For example, both inhibition of actin polymerization (with latrunculin A) and increased actin polymerization (with jasplakinolide) resulted in decreased back intensity. This suggested that the front is at an optimal level of activity to trigger maximal back activation, potentially because low levels of front are necessary to stimulate back, but high levels inhibit back. This is consistent with previous experiments showing that leading-edge activities are globally required for back activation (Pestonjamasp et al., 2006; Van Keymeulen et al., 2006) but also inhibit back activation (Weiner et al., 2006; Xu et al., 2003). These dual roles are analogous to the inositol triphosphate (IP3) receptor calcium channel, which is activated at low levels of calcium but is inhibited by high levels of calcium (Bezprozvanny et al., 1991; Finch et al., 1991). For the IP3 receptor, these dual inputs play an important role in regulating the spatial and temporal dynamics of calcium waves, and such dual interactions could serve a similar function in sculpting the back of polarized neutrophils.

From Network Crosstalk to Causal Networks

Finally, we constructed ''causal networks'' (Sachs et al., 2005) to reveal crosstalk during different phases of the polarization process. For each phenotype, we combined all crosstalk diagrams from individual perturbations to obtain causal networks for each of the five time intervals. Here, we combined perturbations via maximal projection to capture all observed influences between modules (Supplemental Information; Figure S3). We next chose to merge several of these five time intervals to align our analysis with three commonly observed phases of the polarization process: initiation (0–1 min), during which time the cortical burst of F-actin occurs; establishment (1–5 min), during which time front/back polarity is being established; and maintenance (5–10 min), during which time polarity is largely stabilized. The resulting three causal networks were obtained by combining the causal networks in the appropriate time intervals via averaging to reduce noise. (Other approaches for constructing these causal networks, such as obtaining deviation profiles by combining replicate data via medians or means, determining crosstalk links via different z score thresholds, or combining causal networks from different time intervals via an average or minimum of the z scores, also

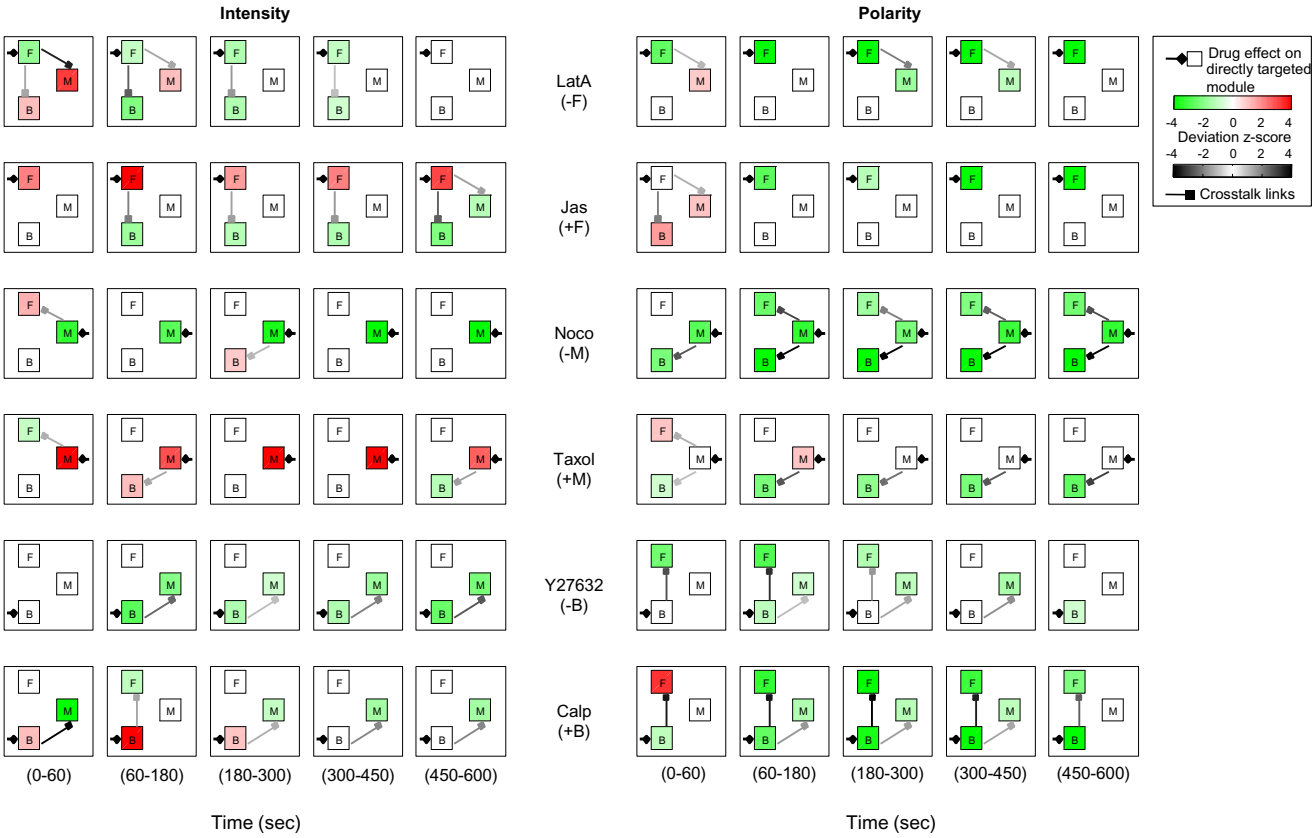

Figure 4. Dynamic Crosstalk in Perturbed Neutrophil Polarity Signaling Networks

Crosstalk diagrams were constructed by analyzing deviations to each of the signaling modules (F, front module; M, microtubule module; B, back module) for each drug perturbation, phenotype, and time interval. Color map for the signaling modules: red (increased intensity/polarity), white (unchanged), and green (decreased intensity/polarity). Diamond arrows represent drug perturbation to the targeted module. Square arrows represent crosstalk from directly to nondirectly targeted modules. Square arrows were colored to reflect the strength of drug effects (bright/dark gray, weak/strong deviation). Left column shows intensity phenotype. Right column shows polarity phenotype. Crosstalk links with small deviations (z score < 1) are not shown.
See also Figure S3.

gave similar results; Supplemental Information; Figures S3 and S4.) The resulting causal networks revealed striking changes in how intensity and polarity crosstalk evolved over time (Figure 5A).

When examining all potential pairs of interactions among modules, we observed that, throughout the polarization process, front-to-back crosstalk persisted for intensity, but not for polarity, phenotypes. In contrast, back-to-front crosstalk persisted for polarity, but not for intensity, phenotypes (consistent with Figure 2B). Microtubule-to-front/back crosstalk was relatively static for polarity but evolved dynamically for intensity (microtubule perturbations affected the front early on, then switched to affecting the back during establishment, and finally affected neither the front nor the back during the maintenance phase). Finally, persistent front/back-to-microtubule crosstalk was observed for intensity (though mostly via the back module) but was absent by the maintenance phase for polarity. We next investigated two properties of the causal networks: first, some modules appeared more insulated from crosstalk than others; second, some crosstalk links were more persistent than others.

Insulation in the Causal Networks

The direction of crosstalk in these causal networks and our previous observations of the deviation profiles (Figure 3C) suggested that the intensity phenotype of the front module after the initiation phase or the polarity phenotype of the microtubule module during the maintenance phase should be insulated from (i.e., not significantly affected by) perturbations to the other modules (Figures 5A and S4, blue squares). To test this prediction, we used double-drug perturbations to simultaneously disrupt both noninsulated modules (Figure 5B, blue squares). We only used combinations of inhibitors/destabilizers, as their indirect effects were more pronounced than enhancers/stabilizers (Figure 4). As predicted by the causal network diagrams based on single-drug perturbation studies, front intensity was insulated from indirect and combined perturbations after the initiation phase (Figure 5B, upper-left). For microtubules, polarity was also insulated from combined front and back perturbations during the maintenance phase (Figure 5B, lower-right). However, this insulation was also observed during the initial and establishment phases, which could be due to synergistic effects of

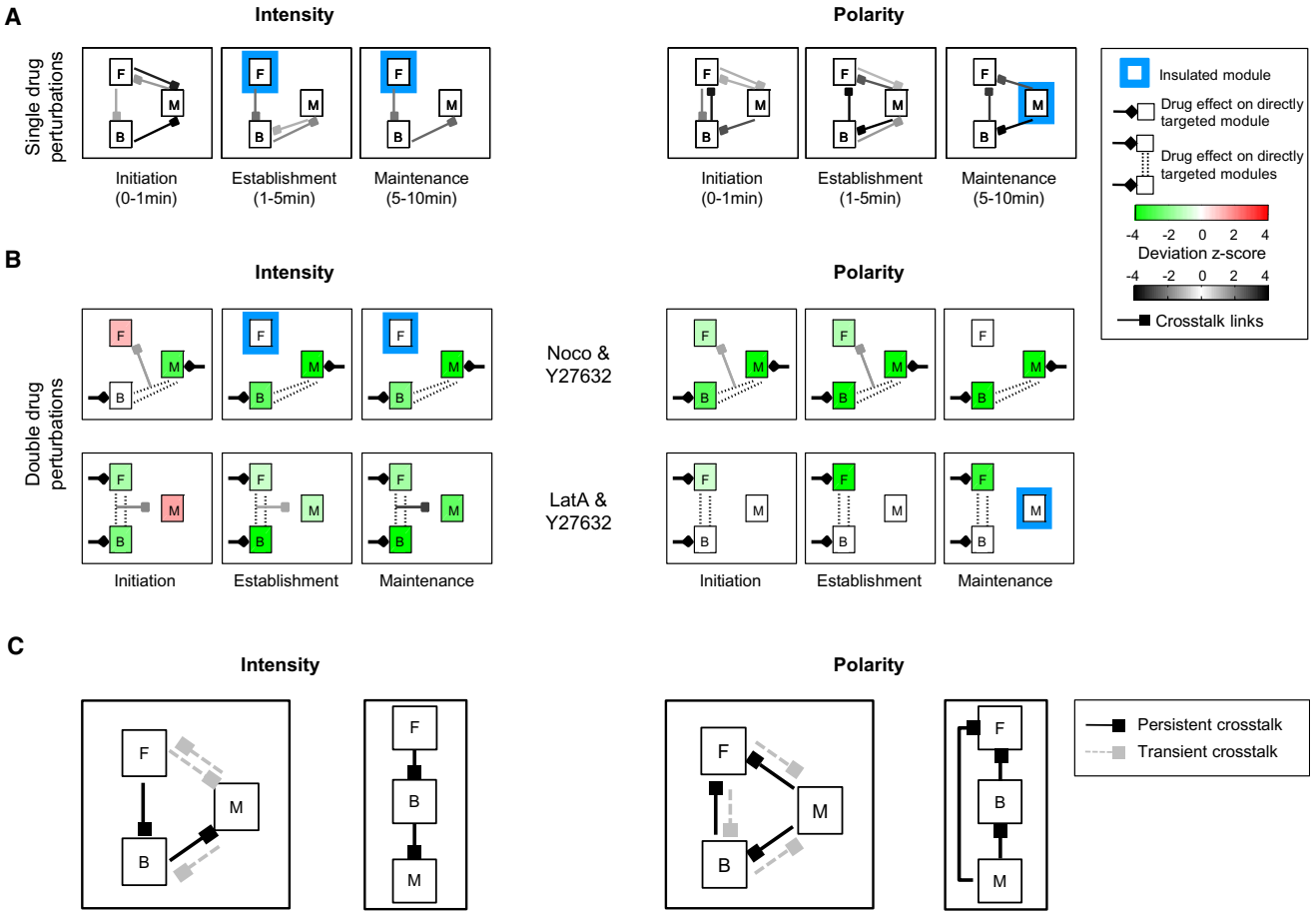

Figure 5. Causal Networks Revealed Dynamic, Phenotype-Dependent Crosstalk with Persistent Interactions Arranged in a Simple Configuration

(A) Causal networks across different stages of polarization (initiation, establishment, and maintenance) were constructed by combining crosstalk diagrams across perturbations and time intervals (Supplemental Information). Square arrows represent crosstalk from directly to nondirectly targeted modules. As in Figure 4, crosstalk with small deviations (z score < 1) is not shown. Blue square represents insulated module.

(B) Crosstalk diagrams obtained from double-drug perturbation assays. Double-dashed lines indicate both direct drug targets. Top row, Noco and Y27632; bottom row, LatA and Y27632. Arrows and color map are shown as in Figure 4.

(C) Summary of all crosstalk links in the causal networks for intensity (left) and polarity (right) phenotypes. Solid/dotted link shows persistent/transient crosstalk. Network motifs that are obtained from persistent crosstalk between modules are shown to the right of the summarized crosstalk diagrams.

See also Figure S4.

combined front/back disruptions. In contrast, and as would be expected from the causal networks (Figure 5A), microtubule intensity and front polarity were vulnerable to combined perturbations of the other modules (Figure 5B, lower-left and upper-right). These crosstalk patterns were consistently observed for different choices of significance thresholds on the deviation z scores (Figure S4B). These results were consistent with predictions of the directionality of crosstalk in the neutrophil polarity network.

Persistent Crosstalk

We next identified crosstalk links in the causal networks that persisted over time (Figure 5C). Surprisingly, crosstalk moved in opposite directions for intensity and polarity phenotypes, particularly during the maintenance phase. Crosstalk persistently originated from the front module for intensity and from the microtubule module for polarity. The persistent links revealed an underlying simplicity of crosstalk influence in the network, namely a linear cascade for intensity and a feed-forward network (Milo et al., 2004) in the opposite direction for polarity (Figure 5C). These two simple, persistent motifs were obscured within the completely connected network that was obtained by combining links from all times and phenotypes.

DISCUSSION

Current efforts to understand signal transduction are focused on two complementary approaches: building extensive and comprehensive catalogs of cellular networks and understanding how complex behaviors arise from these networks. A major challenge is how to connect these two approaches. Here, we show that current knowledge of a network can be leveraged to design

perturbation analyses that allow the dynamics of signal transduction to be inferred directly without a complete biochemical understanding of the entire network.

Although previous studies did not focus on phenotype-specific crosstalk, many of the links that we identified were in agreement with previously identified interactions in the neutrophil polarity network (front to back, front to microtubules, microtubule to back, and back to front). Our analyses also uncovered previously uncharacterized crosstalk interactions in the neutrophil polarity cascade (back to microtubules, microtubules to front) that represent potential starting points for future biochemical investigations. Our approach could be applied in future studies to characterize an expanded set of crosstalk by including additional modules or subdividing the current ones.

Rapid signaling events are typically conceptualized as arising from crosstalk interactions that are unchanging in time. However, we found that this assumption does not hold true for the well-studied process of neutrophil polarization. Crosstalk evolves rapidly during the 600 s period after neutrophil stimulation. What potential mechanisms might underlie these changes? One possibility is that the concentration of components could be changing during the polarization response due to synthesis/degradation, similar to the proteomic changes during different phases of the cell cycle. Alternatively, even static biochemical networks could give rise to changing information flow during different phases of the response due to mechanisms such as time delays or feedbacks. For example, if component A activates component B, and B in turn amplifies its own activity through positive feedback, then initial changes to A should affect the activity of B, but later changes may not. Finally, crosstalk among the modules may be changing due to mechanisms such as post-translational modifications. Future experiments will be necessary to discriminate among different mechanisms of modulating crosstalk.

Intriguingly, the causal network topologies differ depending on the phenotypes for neutrophils. Identifying links that were persistently present for each phenotype revealed a surprising simplicity: a linear cascade underlies the levels of signaling activities, whereas a feed-forward network in the opposite direction underlies the spatial distribution of signaling activities. These phenotype-dependent paths of crosstalk could help explain neutrophils' remarkable chemotactic abilities. For efficient directional migration in the face of subtle external gradients, cells need a mechanism of integrating signals over time to combat the noisy instantaneous receptor-binding events that occur at any given moment in time. One mechanism of integration is for cells to respond to not just the instantaneous receptor occupancy, but also to their recent history by having, for instance, cell response biased by existing polarity (Zigmond et al., 1981). For neutrophils, actin assembly is one of the primary activities that is activated immediately downstream of receptor activation. Based on our experiments, the front module regulates the activities of the back and microtubule modules in a linear cascade that is well suited to read out the current external ligand distribution. To force integration over longer time periods, the microtubule and back modules then set the spatial polarity of the leading edge in a feed-forward loop that is well suited to filter noise and ensure that the leading-edge signaling responds to only the persistent distribution of myosin and microtubules.

How cells process signals is a central question in biology (Amit et al., 2009; Muzzey et al., 2009; Pe'er and Hacohen, 2011). Simple network motifs that represent core causal influences can lie hidden beneath comprehensive, "everything-connects-to-everything" networks that are obtained by combining links from many times and phenotypes. Attempts to superimpose diverse experimental results onto a single topology could lead to overly complex network diagrams and incorrect interpretation of epistatic or feedback relations for complex signaling processes like cell polarization. Our approach for investigating time and phenotype-specific organization of signaling networks through perturbation analysis is general and can be applied more broadly to investigate signal transduction networks beyond our current focus on leukocytes.

EXPERIMENTAL PROCEDURES

Detailed methods can also be found in Supplemental Information.

Isolation of Primary Neutrophils from Human Blood

Human neutrophils were isolated as described in Böyum (1968). In brief, neutrophils from venous blood of a single healthy donor were purified by dextran sedimentation and density-gradient centrifugation with Ficoll (GE health care, 17-5442-02). Contaminating red blood cells were removed by hypotonic lysis.

Choice of Drug Perturbations

To perturb different modules in the neutrophil polarity network, we made use of a set of pharmacological compounds that targeted front (jasplakinolide, latrunculin A), microtubule (taxol, nocodazole), or back (calpeptin, Y27632) modules positively or negatively (Figure 1A). Drug concentrations were chosen by serial titration assays to be strong enough to induce a noticeable effect on primary target activity yet sufficiently small to minimize cytotoxic effects. The drug concentrations were chosen largely to be in the same ranges as values reported in the literature (Figures S1B–1D; Supplemental Information). The same individual drug concentrations were used when we combined pairs of drugs to test their simultaneous effects on neutrophil polarity, i.e., front and back modules (LatA and Y27632) and microtubules and back modules (Noco and Y27632).

Chemotactic Assay for Drug-Treated Cells

Purified human neutrophils were plated into a 96-well Nunc glass plate (Fisher, 12-566-35) and precoated with fibronectin (BD Bioscience, 354008) at a density of ~10,000 cells per well. Cells were incubated at 37°C with 5% CO_2 for 20 min before adding drugs. The concentrations for each drug were as follows: 50 nM for latrunculin A (LatA) (Sigma, L5163), 0.4 μM for jasplakinolide (Jas) (Sigma, C5231), 9 μM for nocodazole (Noco) (Sigma, M1404), 5 μM for taxol (Taxol) (Sigma, T1912), 25 μM for Y27632 (Y27632) (Sigma, Y0503), and 2 μg/μl for calpeptin (Calp) (Cytoskeleton, CN01-A) (Figure S1C). Each drug experiment had two or more repeats that were performed on at least two different days (Noco, n = 6; Taxol, n = 3; LatA, n = 3; Jas, n = 3; Y27632, n = 3; Calp, n = 2; LatA and Y27632, n = 3; Noco and Y27632, n = 2; controls, n = 20). Each repeat experiment consisted of two technical replicates in separate wells that were pooled together for subsequent analysis. After incubation with drugs or control (DMSO) for 30 min at room temperature (RT), cells were simultaneously stimulated with uniform fMLP (10 nM) at 37°C before formaldehyde fixation at different time points ranging from 0–600 s (e.g., 0, 15, 30, 45, 60, 90, 120, 180, 300, 450, and 600 s).

Immunofluorescence Assay

Human neutrophils were fixed and permeabilized after fMLP stimulation. Marker multiplexing was performed as follows. The primary antibodies,

anti-p-MLC2 (Cell Signaling Technology, 3675) and anti-α-tubulin (Cell Signaling Technology, 2144), were added to each well for overnight incubation at 4°C. After three washes, cells were incubated with secondary antibodies conjugated with Alexa 488 (Invitrogen, A11055) and Alexa 546 (Invitrogen, A10040) for 2 hr at RT to fluorescently label p-MLC2 and α-tubulin, respectively. To label F-actin and DNA, cells were incubated with Alexa-647-conjugated phalloidin (Invitrogen, A22287) and Hoechst 33342 (Invitrogen, H1399), respectively, for 30 min at RT followed by three washes.

Image Acquisition for Fixed Cells Assay

All fluorescence images were acquired by using a BD Pathway 855 Bioimager (BD Biosciences) equipped with laser autofocus system, Olympus 40× objective lens, and high-resolution Hamamatsu ORCA ER charge-coupled device (CCD) camera using 1×1 camera binning. Image acquisition was controlled by AttoVision v1.5 (BD Biosciences).

Data Analysis

Image Quality Control

We manually inspected all fluorescence images and discarded those presenting obvious anomalies (e.g., focus issues). Images with poorly segmented cells were resegmented with manually optimized segmentation parameters.

Image Preprocessing and Cellular Identification

Image background subtraction was performed using the National Institutes of Health ImageJ software (Rasband, 1997). Identification of cellular regions and intra- and interplate intensity normalization procedures are discussed in Supplemental Information (see also Ku et al., 2010). The total numbers of cells analyzed in each of the drug conditions are given in Table S1.

Cellular Feature Extraction

For each segmented cellular region, we extracted morphological elongation. Also, for each of the fluorescence readouts (i.e., F-actin for frontness and microtubules and p-MLC2 for backness), we extracted: (1) the average fluorescence intensity (total intensity in the cellular region divided by the cell area) as an integrated readout of the signaling activity of the associated signaling module; and (2) the spatial polarity phenotype, known as compactness, to capture the degree to which the fluorescent readout was spatially concentrated within the cell. Both steps are described in Supplemental Information.

Establishment of Phenotypic Response Curves

For each phenotype, we established the response curve based on cubic interpolation of the population median values collected at different fixation time points. The response curves were smoothed by using the function *fastsmooth.m* downloaded at Matlab Central (http://www.mathworks.com/matlabcentral/fileexchange/19998-fast-smoothing-function). We estimated the variation of the control response curve by the SD among the control median response curves across replicates experiments (Figure S2C, light-gray shaded region). For the drug-treated conditions, variation of the median response curve at each fixation time point was estimated by the SEM among replicate response curves (Figures S2C, second to fourth rows).

Quantification of Drug-Induced Phenotypic Deviation over Time

To estimate the drug-induced deviation of a phenotypic response curve during polarization, for each phenotype f, drug response d, and time interval T (E, EI, I, IL, or L), dimensionless z scores were computed as given in Supplemental Information. The vector of z scores, $\underline{z}^{(f,d)}$, describing temporal evolution of the deviation of response curve was termed a "deviation profile":

$$\underline{z}^{(f,d)} = \left[z_E^{(f,d)} z_{EI}^{(f,d)} z_I^{(f,d)} z_{IL}^{(f,d)} z_L^{(f,d)} \right].$$

Categorization of Deviation Profiles

To categorize deviation profiles with different patterns, we thresholded the z scores. The magnitude of a deviation z score was compared against a numerical threshold τ ($\tau = 1$ in our study) and mapped to 0 if its absolute value was smaller than τ. Upon transformation of the deviation z scores, we categorized the deviation profiles based on their dynamic patterns and further grouped them according to their ability to return to the control level at the end of the polarization process (Figure 3B; Supplemental Information).

Visualization of Network Crosstalk

For a given drug perturbation d and phenotype f, we considered that a crosstalk link existed from the directly targeted module m_1 to a nondirectly targeted module m_2 during the time interval t if the deviation z score $z_t^{(f,d)}$ of module m_2 exceeded a specified threshold τ (i.e., $|z_t^{(f,d)}| > \tau$) (Figure 4).

Construction of Causal Networks

We combined crosstalk observed across multiple drug perturbations by using maximum projection; that is, the maximum amplitude of crosstalk between any pair of signaling modules was kept as the final crosstalk strength (Figure S3; Supplemental Information). To merge crosstalk diagrams associated to different time intervals, we computed average crosstalk strength (Figures 5A, 5B, and S4; Supplemental Information).

SUPPLEMENTAL INFORMATION

Supplemental Information includes Extended Experimental Procedures, four figures, and two tables and can be found with this article online at doi:10.1016/j.cell.2012.03.044.

ACKNOWLEDGMENTS

We thank Neal Alto, Al Gilman, Sasha Jilkine, David Mangelsdorf, Benjamin Pavie, Rama Ranganathan, Mike Rosen, and all other members of the Altschuler, Weiner, and Wu labs. O.D.W. was supported by NIH GM084040 and the Searle Scholars Foundation. L.F.W. and S.J.A. were supported by the Endowed Scholars Program at UTSW Medical Center. L.F.W. was supported by NIH GM081549 and the Welch Foundation I-1644. S.J.A. was supported by NIH GM071794, the Welch Foundation I-1619, and the Rita Allen Foundation.

Received: July 26, 2011
Revised: November 29, 2011
Accepted: March 21, 2012
Published: May 24, 2012

REFERENCES

Amit, I., Garber, M., Chevrier, N., Leite, A.P., Donner, Y., Eisenhaure, T., Guttman, M., Grenier, J.K., Li, W., Zuk, O., et al. (2009). Unbiased reconstruction of a mammalian transcriptional network mediating pathogen responses. Science *326*, 257–263.

Bezprozvanny, I., Watras, J., and Ehrlich, B.E. (1991). Bell-shaped calcium-response curves of Ins(1,4,5)P3- and calcium-gated channels from endoplasmic reticulum of cerebellum. Nature *351*, 751–754.

Böyum, A. (1968). Isolation of mononuclear cells and granulocytes from human blood. Isolation of monuclear cells by one centrifugation, and of granulocytes by combining centrifugation and sedimentation at 1 g. Scand. J. Clin. Lab. Invest. Suppl. *97*, 77–89.

Cheong, R., Rhee, A., Wang, C.J., Nemenman, I., and Levchenko, A. (2011). Information transduction capacity of noisy biochemical signaling networks. Science *334*, 354–358.

de Lichtenberg, U., Jensen, L.J., Brunak, S., and Bork, P. (2005). Dynamic complex formation during the yeast cell cycle. Science *307*, 724–727.

Eddy, R.J., Pierini, L.M., and Maxfield, F.R. (2002). Microtubule asymmetry during neutrophil polarization and migration. Mol. Biol. Cell *13*, 4470–4483.

Finch, E.A., Turner, T.J., and Goldin, S.M. (1991). Calcium as a coagonist of inositol 1,4,5-trisphosphate-induced calcium release. Science *252*, 443–446.

Fraser, I.D., and Germain, R.N. (2009). Navigating the network: signaling cross-talk in hematopoietic cells. Nat. Immunol. *10*, 327–331.

Janes, K.A., Gaudet, S., Albeck, J.G., Nielsen, U.B., Lauffenburger, D.A., and Sorger, P.K. (2006). The response of human epithelial cells to TNF involves an inducible autocrine cascade. Cell *124*, 1225–1239.

Kalir, S., and Alon, U. (2004). Using a quantitative blueprint to reprogram the dynamics of the flagella gene network. Cell *117*, 713–720.

Kentner, D., and Sourjik, V. (2009). Dynamic map of protein interactions in the Escherichia coli chemotaxis pathway. Mol. Syst. Biol. *5*, 238.

Krendel, M., Zenke, F.T., and Bokoch, G.M. (2002). Nucleotide exchange factor GEF-H1 mediates cross-talk between microtubules and the actin cytoskeleton. Nat. Cell Biol. *4*, 294–301.

Ku, C.J., Wang, Y., Pavie, B., Altschuler, S.J., and Wu, L.F. (2010). On identifying information from image-based spatial polarity phenotypes in neutrophils. Proceedings of the IEEE International Symposium on Biomedical Imaging, 14–17, 1029–1032.

Lee, E., Salic, A., Krüger, R., Heinrich, R., and Kirschner, M.W. (2003). The roles of APC and Axin derived from experimental and theoretical analysis of the Wnt pathway. PLoS Biol. *1*, E10.

Levine, H., Kessler, D.A., and Rappel, W.J. (2006). Directional sensing in eukaryotic chemotaxis: a balanced inactivation model. Proc. Natl. Acad. Sci. USA *103*, 9761–9766.

Loose, M., Swiers, G., and Patient, R. (2007). Transcriptional networks regulating hematopoietic cell fate decisions. Curr. Opin. Hematol. *14*, 307–314.

Luscombe, N.M., Babu, M.M., Yu, H., Snyder, M., Teichmann, S.A., and Gerstein, M. (2004). Genomic analysis of regulatory network dynamics reveals large topological changes. Nature *431*, 308–312.

Marco, E., Wedlich-Soldner, R., Li, R., Altschuler, S.J., and Wu, L.F. (2007). Endocytosis optimizes the dynamic localization of membrane proteins that regulate cortical polarity. Cell *129*, 411–422.

Milo, R., Itzkovitz, S., Kashtan, N., Levitt, R., Shen-Orr, S., Ayzenshtat, I., Sheffer, M., and Alon, U. (2004). Superfamilies of evolved and designed networks. Science *303*, 1538–1542.

Muzzey, D., Gómez-Uribe, C.A., Mettetal, J.T., and van Oudenaarden, A. (2009). A systems-level analysis of perfect adaptation in yeast osmoregulation. Cell *138*, 160–171.

Natarajan, M., Lin, K.M., Hsueh, R.C., Sternweis, P.C., and Ranganathan, R. (2006). A global analysis of cross-talk in a mammalian cellular signalling network. Nat. Cell Biol. *8*, 571–580.

Niggli, V. (2003). Microtubule-disruption-induced and chemotactic-peptide-induced migration of human neutrophils: implications for differential sets of signalling pathways. J. Cell Sci. *116*, 813–822.

Odell, G.M., and Foe, V.E. (2008). An agent-based model contrasts opposite effects of dynamic and stable microtubules on cleavage furrow positioning. J. Cell Biol. *183*, 471–483.

Oleksiuk, O., Jakovljevic, V., Vladimirov, N., Carvalho, R., Paster, E., Ryu, W.S., Meir, Y., Wingreen, N.S., Kollmann, M., and Sourjik, V. (2011). Thermal robustness of signaling in bacterial chemotaxis. Cell *145*, 312–321.

Pe'er, D., and Hacohen, N. (2011). Principles and strategies for developing network models in cancer. Cell *144*, 864–873.

Perlman, Z.E., Slack, M.D., Feng, Y., Mitchison, T.J., Wu, L.F., and Altschuler, S.J. (2004). Multidimensional drug profiling by automated microscopy. Science *306*, 1194–1198.

Pestonjamasp, K.N., Forster, C., Sun, C.X., Gardiner, E.M., Bohl, B., Weiner, O., Bokoch, G.M., and Glogauer, M. (2006). Rac1 links leading edge and uropod events through Rho and myosin activation during chemotaxis. Blood *108*, 2814–2820.

Rasband, W.S. (1997). ImageJ. National Institutes of Health, Bethesda, MD, USA. http://imagej.nih.gov/ij/.

Sachs, K., Perez, O., Pe'er, D., Lauffenburger, D.A., and Nolan, G.P. (2005). Causal protein-signaling networks derived from multiparameter single-cell data. Science *308*, 523–529.

Schliwa, M., Pryzwansky, K.B., and Euteneuer, U. (1982). Centrosome splitting in neutrophils: an unusual phenomenon related to cell activation and motility. Cell *31*, 705–717.

Schneider, I.C., and Haugh, J.M. (2006). Mechanisms of gradient sensing and chemotaxis: conserved pathways, diverse regulation. Cell Cycle *5*, 1130–1134.

Servant, G., Weiner, O.D., Herzmark, P., Balla, T., Sedat, J.W., and Bourne, H.R. (2000). Polarization of chemoattractant receptor signaling during neutrophil chemotaxis. Science *287*, 1037–1040.

Small, J.V., Geiger, B., Kaverina, I., and Bershadsky, A. (2002). How do microtubules guide migrating cells? Nat. Rev. Mol. Cell Biol. *3*, 957–964.

Srinivasan, S., Wang, F., Glavas, S., Ott, A., Hofmann, F., Aktories, K., Kalman, D., and Bourne, H.R. (2003). Rac and Cdc42 play distinct roles in regulating PI(3,4,5)P3 and polarity during neutrophil chemotaxis. J. Cell Biol. *160*, 375–385.

Tkachenko, E., Sabouri-Ghomi, M., Pertz, O., Kim, C., Gutierrez, E., Machacek, M., Groisman, A., Danuser, G., and Ginsberg, M.H. (2011). Protein kinase A governs a RhoA-RhoGDI protrusion-retraction pacemaker in migrating cells. Nat. Cell Biol. *13*, 660–667.

Van Keymeulen, A., Wong, K., Knight, Z.A., Govaerts, C., Hahn, K.M., Shokat, K.M., and Bourne, H.R. (2006). To stabilize neutrophil polarity, PIP3 and Cdc42 augment RhoA activity at the back as well as signals at the front. J. Cell Biol. *174*, 437–445.

Weiner, O.D., Neilsen, P.O., Prestwich, G.D., Kirschner, M.W., Cantley, L.C., and Bourne, H.R. (2002). A PtdInsP(3)- and Rho GTPase-mediated positive feedback loop regulates neutrophil polarity. Nat. Cell Biol. *4*, 509–513.

Weiner, O.D., Rentel, M.C., Ott, A., Brown, G.E., Jedrychowski, M., Yaffe, M.B., Gygi, S.P., Cantley, L.C., Bourne, H.R., and Kirschner, M.W. (2006). Hem-1 complexes are essential for Rac activation, actin polymerization, and myosin regulation during neutrophil chemotaxis. PLoS Biol. *4*, e38.

Weiner, O.D., Marganski, W.A., Wu, L.F., Altschuler, S.J., and Kirschner, M.W. (2007). An actin-based wave generator organizes cell motility. PLoS Biol. *5*, e221.

Wong, K., Pertz, O., Hahn, K., and Bourne, H. (2006). Neutrophil polarization: spatiotemporal dynamics of RhoA activity support a self-organizing mechanism. Proc. Natl. Acad. Sci. USA *103*, 3639–3644.

Wong, K., Van Keymeulen, A., and Bourne, H.R. (2007). PDZRhoGEF and myosin II localize RhoA activity to the back of polarizing neutrophil-like cells. J. Cell Biol. *179*, 1141–1148.

Xu, J.S., Wang, F., Van Keymeulen, A., Herzmark, P., Straight, A., Kelly, K., Takuwa, Y., Sugimoto, N., Mitchison, T., and Bourne, H.R. (2003). Divergent signals and cytoskeletal assemblies regulate self-organizing polarity in neutrophils. Cell *114*, 201–214.

Xu, J.S., Wang, F., Van Keymeulen, A., Rentel, M., and Bourne, H.R. (2005). Neutrophil microtubules suppress polarity and enhance directional migration. Proc. Natl. Acad. Sci. USA *102*, 6884–6889.

Yu, R.C., Pesce, C.G., Colman-Lerner, A., Lok, L., Pincus, D., Serra, E., Holl, M., Benjamin, K., Gordon, A., and Brent, R. (2008). Negative feedback that improves information transmission in yeast signalling. Nature *456*, 755–761.

Zigmond, S.H., and Sullivan, S.J. (1979). Sensory adaptation of leukocytes to chemotactic peptides. J. Cell Biol. *82*, 517–527.

Zigmond, S.H., Levitsky, H.I., and Kreel, B.J. (1981). Cell polarity: an examination of its behavioral expression and its consequences for polymorphonuclear leukocyte chemotaxis. J. Cell Biol. *89*, 585–592.